Lead Article

Acta Cryst. (1987). A43, 737–751

The Present and Future of High-Resolution Electron Microscopy*

BY J. M. COWLEY

Department of Physics, Arizona State University, Tempe, Arizona 85287, *USA*

AND DAVID J. SMITH

Center for Solid State Science and Department of Physics, Arizona State University, Tempe, Arizona 85287, *USA*

(*Received* 8 *December* 1986; *accepted* 6 *July* 1987)

Abstract

High-resolution electron microscopy, with the current resolution limits of better than 2 Å, has been proven to be a valuable technique for the study of radiation-resistant crystals, allowing the determination of the structures of perfect crystal regions, crystal defects and crystal surfaces with atomic resolution. As the resolution is improved, however, the image contrast is increasingly determined by dynamical diffraction effects and it is increasingly sensitive to the instrumental parameters and to the geometry and alignment of the specimen. For both the conventional transmission electron microscope and the scanning transmission electron microscope, further developments should lead to better or more versatile performance, up to the limits set by the fundamental problems of radiation damage. Major advances may be expected from developments of the associated techniques of microanalysis and microdiffraction. Applications of particular interest will include studies of surfaces and interfaces, small particles and radiation-induced chemical reactions.

Introduction

High-energy electrons ($E_0 \sim 50$–1000 keV) have extremely short wavelengths ($\lambda_{el} \sim 0{\cdot}05$–$0{\cdot}01$ Å), which raises the prospect that sub-ångström detail might be visible in electron micrographs. In practice, electron lenses have unavoidable aberrations which combine to limit the effective image resolution in contemporary microscopes to around 1–3 Å. Nevertheless, resolving powers of this order mean that it becomes possible directly to resolve individual atomic columns in low-index zone-axes projections of most oxides, metals, ceramics and semiconductors. The technique of high-resolution electron microscopy (HREM) thus represents an invaluable means for characterizing the defect structure of real materials on the atomic scale.

A few examples of recent accomplishments may be quoted in order to illustrate the current capabilities of the method. It was the high-resolution electron micrographs of the quasi-crystalline Al–Mn phase (Bursill & Lin, 1985; Hiraga, Hirabayashi, Inoue & Matsumoto, 1985) which gave the first definitive account of how the icosahedral symmetry is incorporated in an actual structure. The possibility of resolving distinctly the atom columns in semiconductor crystals has allowed valuable information to be obtained on the forms of the silicon/silicide, the silicon/silica and other interfaces of importance for solid-state electronics developments (*e.g.* Hutchison, 1985). The nature of the termination of crystals at surfaces and the mobility of surface atoms in response to various stimuli have been revealed by static and dynamic observations with atomic resolution. Examples include the studies of metal surfaces by Smith & Marks (1985), the studies of oxides by Kang, Smith & Eyring (1986) and the observations of the rapid changes of shape and structure of very small metal particles by Smith, Petford, Wallenberg & Bovin (1986) and Iijima & Ichihashi (1986). Crystallographic structural transformations have been observed and interpreted in terms of atom movements, for example by Eyring, Dufner, Goral & Halladay (1985).

We do not aim, in this article, to provide a review of the accomplishments of HREM beyond these few limited illustrations of its capabilities. Our objective is to review the present status of the techniques and to consider possible directions for future improvements. Our discussion is limited to those non-biological materials which are sufficiently resistant to radiation damage by the incident electron beam to allow useful high-resolution imaging.

* *Editorial note*: This invited paper is one of a series of comprehensive Lead Articles which the Editors invite from time to time on subjects considered to be timely for such treatment.

0108-7673/87/060737-15$01.50

Modes of operation

The two basic configurations for image formation in the transmission electron microscope are represented schematically in Fig. 1. From the principle of reciprocity, they can be considered equivalent (Cowley, 1969).

In conventional transmission electron microscopy (CTEM), a broad, nearly parallel, beam of electrons is incident on the specimen and electrons which are transmitted or scattered by the sample through the objective lens aperture eventually form the final magnified image at the base of the microscope column. Micrographs have traditionally been recorded on films or plates with electron-sensitive emulsion, but there has been a recent trend towards using image pickup systems and videotape recording. Not only can dynamic events on the atomic scale be followed in real time and later analyzed in detail (Smith, 1985), but the image pickup system provides a mechanism whereby computer-controlled adjustment of critical microscope functions becomes feasible (Saxton, Smith & Erasmus, 1983).

In scanning transmission electron microscopy (STEM), a focused beam is scanned across the (thin) specimen and the image is formed by collecting electrons transmitted by the sample. In principle, it is possible to obtain the same contrast and resolution as in CTEM (Cowley, 1969), but the resolution was originally limited in practice by the brightness of the electron gun. The development for STEM of the field emission gun (Crewe, Wall & Welter, 1968), with its source brightness increased by a factor of 10^4 relative to thermionic emission sources, provided an electron source which was sufficiently bright to allow high-resolution images to be recorded in acceptable times (10–20 s). The applications of STEM to the study of crystals have nevertheless been limited in number. This is partly because of the difficulty of obtaining good signal-to-noise ratios for image areas of reasonable size, but primarily because the STEM instruments have been directed towards other applications, described below, which have generally been considered to have more immediate practical value.

Dynamical scattering and transfer function theory

The image formation process in the CTEM can be considered in two distinct parts, namely the dynamical scattering of the electron beam as it is transmitted through the sample, followed by propagation through the objective lens and the magnifying lenses of the microscope. In diffraction- or amplitude-contrast imaging, the objective aperture size is chosen so that only the transmitted and small-angle-scattered electrons contribute to the image. In HREM, many diffracted beams contribute to the image; the spatial filtering effect of the objective lens is then critical to the image formation process.

The simplest approach to electron scattering is to treat the specimen as a weak-phase object (WPO). It is assumed that the electron wave undergoes a phase change in the potential field of the crystal and the total phase change in the specimen is proportional to the potential distribution projected onto a single plane, if one ignores Fresnel diffraction within the sample. This approximation is really only valid for light atoms and very thin specimens, although WPO calculations as a function of resolution provide a useful basis for evaluating defect models. Dynamical scattering depends on the spatial distribution of atoms throughout the depth of the specimen and needs to account for the possibility of multiple scattering and strong phase changes. In the multislice treatment, which has been extensively adopted for computer image simulations (Goodman & Moodie, 1974), the sample is divided into thin slices normal to the beam direction, with the atoms in each slice projected onto a single plane (Cowley & Moodie, 1957). The electron distribution emerging from each slice is propagated by Fresnel diffraction and taken as the new input for the next slice. The process is repeated until the last slice is reached and the final electron distribution represents the exit-surface wavefunction which is then propagated through the rest of the microscope. More details of these and other approaches to dynamical scattering theory can be found elsewhere (Cowley, 1981).

The effect on the image wave function of the lens aberrations and aperture is best described in terms of the transfer function (TF). This function modifies the amplitudes of the diffraction pattern, formed in the back-focal plane of the objective lens. It includes the limitations on the range of diffraction angles by the objective aperture and also the phase changes resulting from defocus and the lens aberrations. The wave function for the image is then given by Fourier transform of the product of the diffraction amplitude function by the TF; that is, by the convolution of the exit wave function from the object with the spread function, which is the Fourier transform of the TF. The spread function represents the limitation on resolution and the distortion of image intensities.

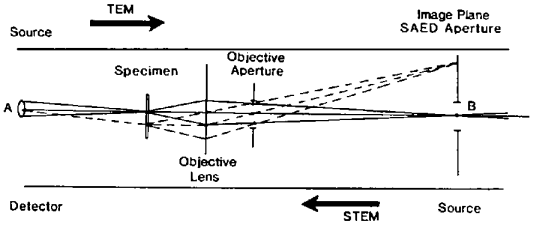

Fig. 1. Diagram of the objective-lens action for CTEM (electrons travelling from left to right) and for STEM (electrons travelling from right to left).

The TF is specimen-independent and it can be represented in generalized units, making it a simple matter to compare microscopes operating at different voltages or having different objective-lens characteristics. The TF also provides a convenient means for understanding the resolution limits associated with different imaging modes, and hence it can be useful for discussing resolution improvements (see later).

The two-dimensional vector in the diffraction patterns $\mathbf{u}$, coordinates u, v has magnitude $|\mathbf{u}| = (2\sin\theta)/\lambda$, where θ is half the scattering angle. The generalized spatial frequency is $k = |\mathbf{u}|/(C_s\lambda^3)^{1/4}$ and the generalized objective lens defocus is $D = \Delta f/(C_s\lambda)^{1/2}$, where Δf is the defect of focus. In the ideal case of a weak-phase object (WPO) and coherent axial illumination, the TF may be replaced by the phase-object transfer function (PCTF),

$$T(k) = 2\sin\gamma(k) = 2\sin\pi k^2(k^2/2 - D). \quad (1)$$

This PCTF multiplies the amplitudes of the diffraction pattern in the back-focal plane of the lens. Fourier transformation of the product then gives the variations of intensity in the image. The PCTF drawn as a solid line in Fig. 2 corresponds to a 500 keV HREM with a spherical aberration coefficient (C_s) of 2·0 mm, at the generalized defocus $D = (1{\cdot}5)^{1/2}$, the so-called first broad-band position. This curve, which has the same shape for *all* C_s and λ at this specific defocus, becomes increasingly oscillatory at higher spatial frequencies (corresponding to higher resolution). Electrons scattered to higher angles thus suffer phase reversals which could lead to artefactual detail of opposite contrast appearing in the final image. Finally, note the strong focal dependence in (1) which also results in phase reversals and further image artefacts at other defoci.

In practice, instrumental factors normally limit the temporal (energy spread) and spatial (angular spread) coherence of the electron beam, resulting in attenuation of the ideal PCTF at higher spatial frequency. Such partial coherence of the illumination almost invariably imposes the decisive limitation on the image resolution. HREMs operating at 100 or 200 keV have generally been limited by spatial coherence, while higher-voltage microscopes are usually limited by chromatic effects (Smith, Camps & Freeman, 1982). The curve B in Fig. 2 shows the damping of the PCTF which results from an incident-beam semi-angle of 0·4 mrad and a focal spread of 100 Å.

A representation of the effects of partial coherence, in the form of envelope functions which multiply the ideal PCTF, has been developed (Frank, 1973; Saxton, 1978). The spatial coherence envelope is given by

$$B(k) = \exp[-\pi^2 s^2 k^2 (k^2 - D)^2], \quad (2)$$

where s is a generalized angular coordinate representing the illumination divergence. The two families of curves in Fig. 3 compare the damping effects of increased beam divergence as functions of scattering angle for the generalized defocus values $D = 1$ (Scherzer focus) and $D = 3^{1/2}$ (second broad band). The temporal coherence envelope is given by

$$C(k) = \exp[-\pi^2 d_0 k^2/2] \quad (3)$$

where d_0 is a measure of the effective half-width of the energy-spread distribution, and includes contributions from the intrinsic energy spread of the electrons emitted by the source, as well as high voltage and lens-current instabilities. Note that the spatial coherence envelope is focus dependent, unlike that for temporal coherence: the difference provides a practical means of distinguishing between the two effects.

It must be emphasized that the envelope functions, like the PCTF, can be applied only for weak-phase objects and are not applicable for most images of crystals. For most inorganic crystals, the weak-phase object approximation (WPOA) fails for even very thin samples and more complicated considerations apply.

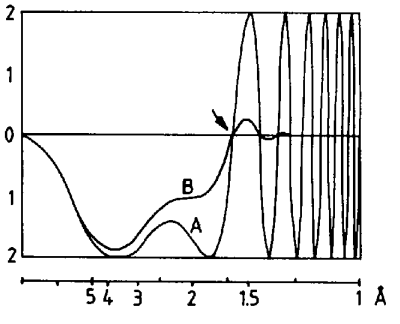

Fig. 2. Theoretical CTF curves for optimum objective-lens defocus. Curve *A*: fully coherent illumination; curve *B*: partially coherent illumination. $V_A = 500$ kV; $C_s = 2{\cdot}0$ mm; focal spread = 100 Å; incident-beam half-angle = 0·4 mrad.

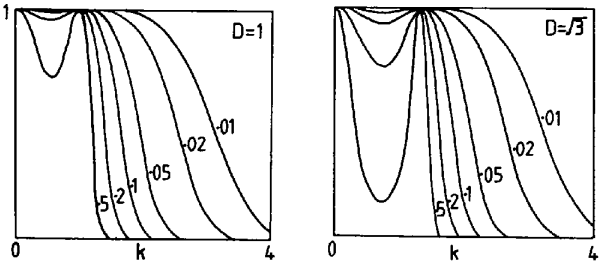

Fig. 3. Spatial coherence envelopes at two defocus values as a function of generalized spatial frequency $k(= C_s^{1/4}\lambda^{3/4})$ showing the dampening effect of increasing the beam divergence s.

Resolution criteria and optical diffractograms

There are several commonly used definitions of resolution which need to be distinguished. The interpretable resolution is related to the widest possible interval for the transfer of specimen information with constant phase, under axial illumination conditions, for a weak-phase object. This resolution limit is given by $\delta \sim 0{\cdot}66 C_s^{1/4} \lambda^{3/4}$ and it roughly corresponds to the position, arrowed in Fig. 2, where the PCTF curve first crosses the horizontal axis. This *interpretable* resolution is now the quantity, generally referred to as the *resolution*, which indicates the scale of information which can be directly inferred by observing the image. It has replaced the poorly defined term *point-to-point* resolution, which is based on concepts inappropriate for coherent image formation in an electron microscope. The *instrumental* resolution describes the limitation on the fineness of detail which can be produced in an image, irrespective of whether it can be related to object detail or not. It is governed by the various damping functions, which can include the effects of mechanical vibrations as well as the partial coherence envelopes described above. The normally accepted criterion is a $1/e^2$ reduction in the magnitude of the PCTF. This particular limit is focus dependent because of the occurrence of D in (2), and also thickness dependent because, with increasing thickness, the limitations of (2) and (3) are modified by multiple-scattering effects. Finally, the *line* or *lattice-fringe* resolution corresponds to the finest spacing of lattice fringes visible in the image. These fringes involve interference between two specific diffracted beams, often recorded with tilted illumination to minimize chromatic effects. The lattice-fringe resolution is basically a reflection of instrumental stability but it is not a useful measure of the finest local information about the sample which can be extracted from the electron micrograph.

A determination of the transfer function for a particular microscope is usually necessary before the instrument can be utilized effectively for obtaining quantitative structural information. It must be applied in any process of image matching used to test postulated structural models. Essential instrumental parameters can be found by making careful comparison between computer image simulations and a through-focal series of experimental micrographs from a known test object (Wilson, Spargo & Smith, 1981). It is often more practicable, however, to record images from a thin sample of an amorphous material such as silicon. These micrographs are placed in a light-optical bench, or diffractometer, and the (Fourier) transforms of the image intensity, called the optical diffractograms, can then be analyzed to provide the required information about the imaging properties of the microscope following the method of Thon (1971), described by Erickson (1973). From the diffractograms from a focal series of images, it is possible to determine the C_s value, the size of the focal steps, the amount of objective-lens astigmatism, the focal spread and the effective illumination angle. Many HREM laboratories these days contain simple light-optical benches in order to facilitate this process of diffractogram analysis: When possible, it is preferable to use an on-line computer system to obtain the Fourier transform of a digitized image. This can be very fast and allows the stigmation and defocus to be checked before, rather than after, recording the image.

Image interpretation and simulations

The main objective of high-resolution electron microscopy is to relate the fine details of the electron micrograph in a meaningful way to the morphological features of the sample under observation. There are many cases in which images of thin crystals show directly, and clearly, the relative positions of atoms in the projection of a crystal structure (see Fig. 4). However, even with the best modern microscopes it is not in general possible to achieve a straightforward interpretation of images, given the rapid variation of image detail with both defocus and specimen thickness, and the sensitivity to instrumental parameters, particularly the high voltage and C_s value. Moreover, with the recent improvements in microscope performance it is becoming increasingly difficult for even highly experienced operators to optimize the instrumental adjustments with sufficient precision (Smith, Saxton, O'Keefe, Wood & Stobbs, 1983). For these reasons image simulations, based on dynamical scattering and TF theory, are regarded as an essential part of quantitative HREM studies. Computer programs based on the multi-slice formulation of n-beam

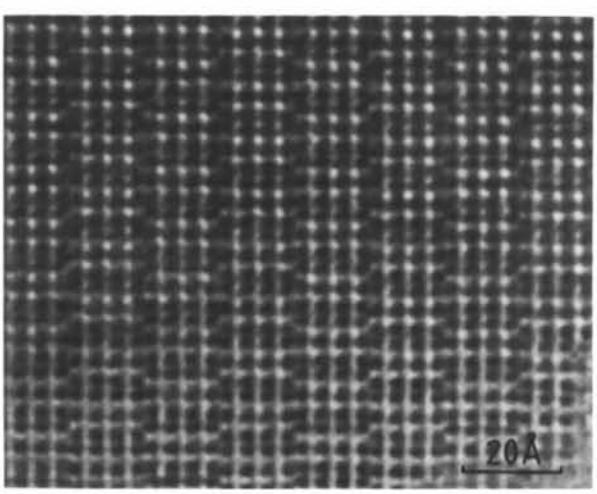

Fig. 4. Crystal structure image of $Ti_2Nb_{10}O_{29}$ recorded at 400 kV with an interpretable resolution limit of ~1·7 Å. Each black spot represents a row of cations viewed end-on.

dynamical theory (Cowley & Moodie, 1957) are nowadays well established (Goodman & Moodie, 1974; Self, O'Keefe, Spargo & Buseck, 1984). The elimination of alternative models for the structure of defects is often possible by a comparison of experimental micrographs with computed images of these defects (Smith, Bursill & Wood, 1983).

The computer programs now available are generally considered to give accurate representations of the scattering of electrons by thin crystals, and can be extended to describe the diffraction and imaging of defects. Provided that reasonable precautions are taken, it is possible to ensure accuracies of a few percent, or better than the probable error limits of experimental observation. Reservations must be expressed, however, when applications are made to scattering by crystals more than 200–300 Å thick. No adequate provision is made for the inelastic scattering effects, either in the calculation of the contributions of the inelastically scattered electrons to the image intensities or in the modifications of the elastic-scattering processes to take account of absorption effects associated with inelastic scattering. These and other more subtle effects must be properly treated before it is possible to make accurate quantitative comparisons for images from thicker crystals. The incentive to use thicker-crystal images arises because they contain inherently more information than thin-crystal images. They are more strongly influenced by small atom displacements, bonding and valence states of atoms and thermal vibration parameters.

Applications of the STEM

Imaging modes

When the very small very bright electron probe (diameter as small as 5 Å or less) of the STEM instrument is scanned over a specimen, an image of the sample may be obtained by collecting any one of a large number of resultant signals. Multiple images may be formed by utilizing more than one of these signals simultaneously.

The available signals include: (*a*) Electrons transmitted without energy loss, giving a bright-field image due to (small-angle) elastic scattering; (*b*) Electrons transmitted with energy losses due to inelastic-scattering processes, detected by use of an electron energy-loss spectrometer (EELS); (*c*) Electrons scattered elastically (or inelastically) outside the directly transmitted electron beam. Detection of these scattered electrons by the use of an annular detector gives an annular dark-field STEM image. Detection of a particular diffracted beam gives a dark-field image analogous to the dark-field images obtained with the CTEM; (*d*) Characteristic X-rays from inner-shell excitations of atoms in the specimen, giving images which show the spatial distribution of particular elements; (*e*) Secondary electrons, with energies mostly in the 0–100 eV range; (*f*) Auger electrons, with energies in the range 100–2000 eV, which are characteristic of the emitting atoms; (*g*) Visible light from cathodoluminescent processes; (*h*) Enhanced conductivity of the sample induced by irradiation with the incident electron beam.

The delocalization of the inelastic scattering processes giving rise to the emitted signal in cases (*g*) and (*h*), and to some extent (*b*), (*c*) and (*f*), excludes the possibility of high-resolution imaging. The resolution is usually severely limited by the relative weakness of the signal in cases (*d*), (*f*)–(*h*), and for (*b*) in the case of the inner-shell excitations which are characteristic of the atoms present. It is very difficult to obtain acceptable signal-to-noise ratios except by utilizing large-current, large-diameter incident beams, equivalent to low-resolution conditions. Improvements in detector efficiency in the near future are expected to provide significant improvements in the resolution limits for (*f*) and, to some extent, for (*b*) and (*e*). For other signals, the limitation is more fundamental. Since the detected signal comes from low-energy electrons which have very limited range in solids, the detection in cases (*e*) and (*f*) provides information on the structure of thin surface layers only.

Present resolution limits are about 3 Å for (*a*) and (*c*), 10 Å for (*e*) and for (*b*) with 10–30 eV energy losses, and 100 Å or more for all other signals. Examples of bright-field (BF) and annular dark-field (DF) images from a thin crystal of $Ti_2Nb_{10}O_{29}$ (Cowley, 1984) are shown in Fig. 5. The contrast of the BF image is similar to that observed in CTEM images with a resolution limit of about 4·5 Å. The annular DF image has reversed contrast and the resolution is about 3·5 Å. The improvement in resolution over the BF case is roughly the same as given by the approximate theoretical treatment applicable to thin weakly scattering objects (Cowley & Au, 1978), but inapplicable here.

In Fig. 6 a comparison is made between a BF STEM image and a secondary-electron microscope (SEM) image obtained simultaneously with secondary electrons emitted from the sample. The latter shows clearly the sensitivity to surface morphology with a resolution limit of about 10 Å. Comparable results have been reported by Imeson, Milne, Berger & McMullan (1985).

Although the emphasis of this article is on high-resolution imaging and diffraction, the importance of the capabilities of STEM instruments for the microanalysis of very small regions cannot be ignored. The possibilities of chemical analysis from individual small defect regions is well illustrated by the detection of nitrogen in platelet defects in diamond by Berger & Pennycook (1982) and the detection of oxygen in

small precipitates in silicon by Bourret & Colliex (1982).

Microdiffraction

From the crystallographer's point of view, the most interesting aspect to STEM is that for any position of the incident electron beam on the specimen a diffraction pattern from the illuminated region is formed on any subsequent detection plane (Fig. 7). The diameter of the region illuminated is approximately equal to the resolution limit for annular DF images, currently somewhat less than 3 Å. With an efficient two-dimensional detection system, diffraction patterns from such areas may be recorded at TV rates with good signal-to-noise ratios (Cowley, 1980).

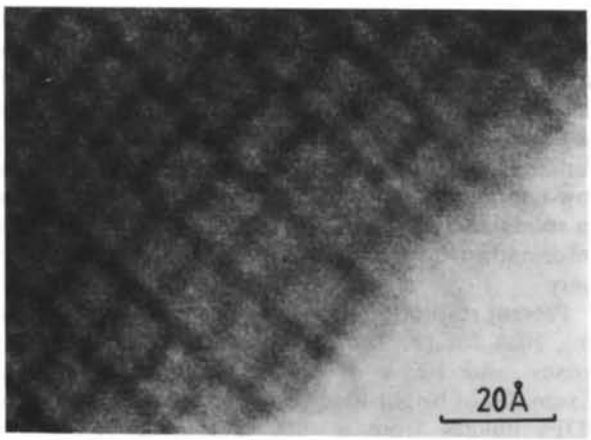

(*a*)

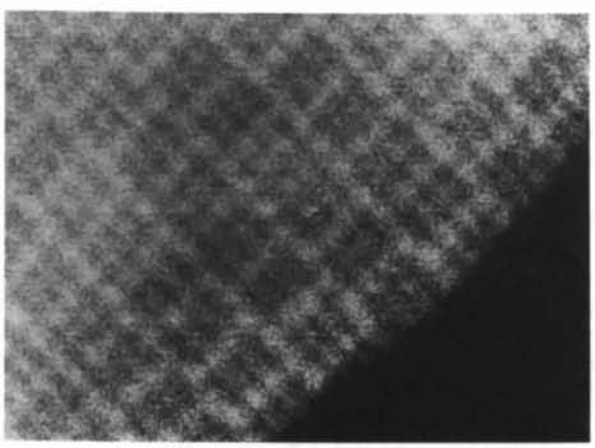

(*b*)

Fig. 5. (*a*) Bright-field STEM image of the thin edge of a crystal of $Ti_2Nb_{10}O_{29}$; apparent resolution about 4·5 Å. (*b*) Dark-field STEM image obtained using the same incident beam with an annular detector; apparent resolution about 3·5 Å (Cowley, 1984).

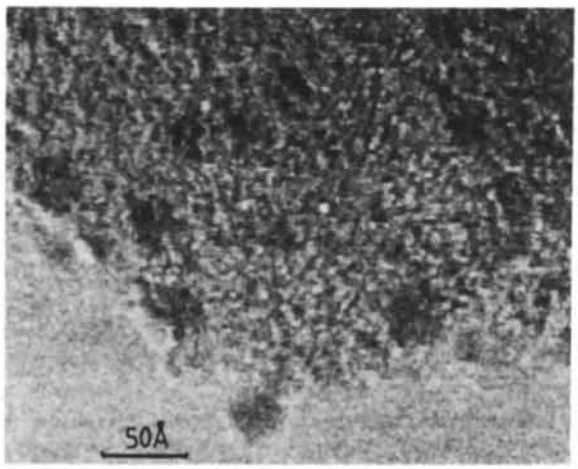

(*a*)

(*b*)

Fig. 6. (*a*) Bright-field STEM image, and (*b*) secondary-electron image of small metal particles (Ru and Au) on an MgO support.

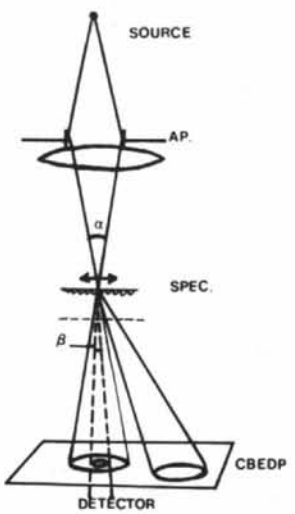

Fig. 7. The use of a convergent beam in a STEM instrument to form a small probe on the specimen and a convergent-beam electron diffraction pattern.

Videotape recordings of diffraction patterns from regions approximately 3 Å in diameter have been obtained as an electron beam was scanned in steps of about 0·2 Å across a planar defect in a thin diamond crystal (Cowley, Osman & Humble, 1984). An interpretation of the defect structure was attempted by comparing diffraction patterns with computations based on many-beam dynamical diffraction theory for various postulated models of the defect.

The diffraction patterns obtained with the probe stationary are convergent-beam diffraction patterns since a relatively large beam convergence angle (of the order of 10^{-2} rad) is needed to define the small probe size (Fig. 7). These patterns do not exhibit distinct diffraction spots when the incident-beam diameter is much smaller than the dimensions of the unit cell projected in the incident-beam direction. The diffraction spots then become overlapping discs with diameters larger than the separations of the parallel-beam spots. Coherent interference between the diffracted beams strongly modifies the intensities in the regions of overlap.

This interference between the overlapping beams means that the diffraction-pattern intensities depend on the relative phases as well as the amplitudes of the diffracted beams. Consequently, there is no 'phase problem' and the diffraction-pattern intensities may in principle be interpreted unambiguously in terms of the absolute positions of atoms relative to the center of the incident beam. However, both the collection of data with adequate specification of the relevant experimental parameters and the interpretation of the observations are by no means trivial. The intensity at any point in the diffraction pattern depends on the location of the incident beam within the projected unit cell (so that a STEM lattice image will be formed as the incident beam is scanned over the specimen). The intensity may also depend strongly and non-linearly on the crystal thickness and tilt, and on the defocus, aberrations and alignment of the objective lens. Finally, the intensities will be modified by any other perturbation of the phases of incident or diffracted beams, for example by any contamination or other amorphous layers on the crystal surfaces, or by any supporting film, even if only 10–20 Å thick.

With sufficient control of specimen preparation and an accurate determination of the relevant experimental parameters, it is possible to envisage a structure analysis from regions which are 3 Å or more in diameter. If sets of diffraction patterns were obtained as the beam was scanned (preferably digitally) over a specimen, then the solution of the structure for one area could be used to assist in the structure determination of the adjacent overlapping areas. A periodicity of the sample, and hence a relatively simple projection, in the beam direction is preferable, but periodicity in other directions is irrelevant. The interpretation of the diffraction patterns would normally be in terms of many-beam dynamical theory since the kinematical scattering approximation is rarely adequate.

A full realization of such a scheme, with structure analysis extending far beyond the resolution limits of electron microscopy, currently appears remote. Initial stages in the exploration of the basic techniques may include the determination of symmetry around particular points within the unit cell of a crystal or in the vicinity of a crystal defect. Fig. 8, for example, was obtained with an incident beam of approximately 4 Å diameter which was stopped within the unit cell of a crystal of $Ti_2Nb_{10}O_{29}$ (*cf.* Fig. 4). The appearance of near-symmetry elements within the pattern suggests that the location of the beam is close to the intersection of two mirror planes in the projection of the structure.

Recently Konnert & D'Antonio (1986) have proposed a technique in which, for each position of the incident beam (*i.e.* for each image pixel), the diffraction pattern is recorded digitally and Fourier transformed to give a Patterson function of the illuminated specimen region. Maxima in the

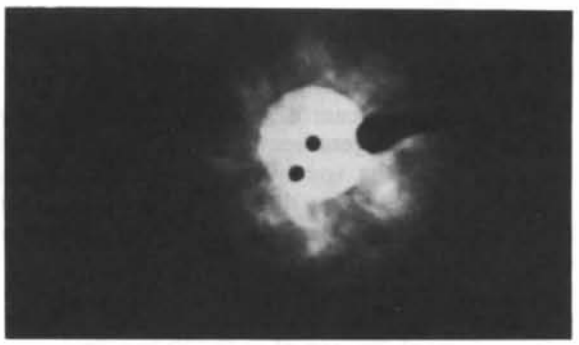

(*a*)

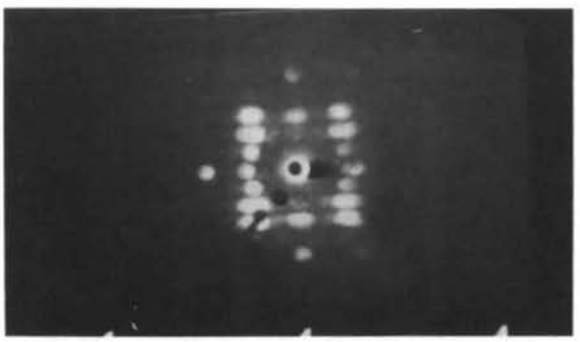

(*b*)

Fig. 8. (*a*) Diffraction pattern in the [010] direction from a region about 4 Å in diameter within the unit cell of a $Ti_2Nb_{10}O_{29}$ crystal ($a = 28{\cdot}5$, $c = 20{\cdot}5$ Å). For comparison, (*b*) is the diffraction pattern from a region about 15 Å in diameter for which the separate diffraction spots are almost resolved. [The black spots are detectors used to collect image signals (Cowley, 1984).]

Patterson function will occur when the center of the electron beam is halfway between atoms, allowing the specimen structure to be derived with improved resolution. The technique involves a large amount of computation but initial tests suggest that useful results may be possible in at least some favorable cases.

A further possible use for these microdiffraction patterns could involve pattern-recognition techniques to locate and correlate patterns originating from particular local atomic configurations (Monosmith & Cowley, 1983). Such procedures may be especially important for the analysis of disordered or near-amorphous samples.

While the utilization of diffraction patterns presents serious practical difficulties for beams of diameter 5 Å or less which are smaller than the dimensions of many unit cells, patterns from larger beams, 10 to 20 Å in diameter, are being routinely applied to many problems, particularly the study of small particles and microcrystalline films (Cowley, 1984). For small-unit-cell materials the diffraction patterns are recognizably well defined spot patterns. The fine structure due to coherent diffraction effects is frequently visible and sometimes useful.

In-line holography

The convergent-beam diffraction patterns formed by coherent convergent beams giving a small crossover at or near the specimen may be regarded as in-line holograms. This description becomes more apparent when a very large objective aperture is used and the diffraction pattern clearly becomes a shadow image of the specimen, distorted by the lens aberrations. In his original paper on holography, Gabor (1948) proposed the use of such shadow images, or holograms, as a means for improving microscope resolution. He suggested the procedure of reconstruction from the hologram by use of a light-optical analog system in which the electron-optical aberrations are corrected.

It has recently become feasible to test this idea by using the field-emission gun of a STEM instrument to form a fine crossover with a coherent convergent beam. The light-optical reconstruction process is then replaced by computer manipulation of a digitized hologram. Some limited success has been achieved with this method (Lin & Cowley, 1986), but there are fundamental and practical limitations which complicate and restrict its use. Existing theory and current techniques limit the application to very thin weakly scattering objects, therby excluding most crystalline specimens. Experimentally, limitations are imposed by the same factors which degrade microscope resolution, namely chromatic-aberration effects due to voltage or current fluctuations and mechanical or electrical instabilities of the instrument.

Off-line holographic techniques, using crystal diffraction for beam splitting, have been explored extensively, for example by Tonomura (1986). These techniques can be effective in studies of magnetic and electrostatic fields but are not appropriate for the enhancement of resolution.

Applications of the CTEM

Imaging modes

Most of the signals which can be utilized for imaging in the STEM are unusable in the CTEM because, without sequential imaging, no spatial discrimination is obtainable. Imaging in the CTEM is therefore effectively restricted to those electrons which are transmitted by the sample. Bright-field or dark-field images respectively are obtained, depending upon whether or not the directly transmitted electron beam contributes to the image. The resolution and contrast of the final CTEM image will depend, among other things, upon the size and position of the objective aperture. In HREM, the coherence envelopes determine the instrumental or interpretable resolution limit, but the objective aperture size is still usually chosen approximately to match this limit so that large-angle inelastically scattered electrons are prevented from lowering the final image contrast.

While most microscopists recognize the necessity for accurate tilting of a crystalline sample, comparatively few really appreciate the consequences of incident-beam (mis)alignment. Off-axis misalignment results in the introduction of antisymmetric phase shifts into the TF which cause lateral displacements of image detail and the loss of any centrosymmetry otherwise present in the image (Smith, Saxton, O'Keefe, Wood & Stobbs, 1983). The problem is accentuated for materials with symmetry elements giving rise to kinematically and dynamically forbidden reflections (Smith, Bursill & Wood, 1985), like the thin crystal of rutile shown in Fig. 9. In the high-excitation objective lenses commonly used nowadays, the traditional current- or voltage-center alignments are usually inadequate because of asymmetric magnetic-field distributions in the vicinity of the objective lens. It is then necessary to resort to other more refined methods [for details see Zemlin, Weiss, Schiske, Kunath & Herrmann (1978) and Smith, Saxton, O'Keefe, Wood & Stobbs (1983)], and the assignment of point groups for an unknown structure should never be done solely on the basis of high-resolution micrographs.

Lattice-fringe and crystal structure imaging

When a thin crystal is tilted so that a low-order diffracted beam is strongly excited, the dynamical interactions of the diffracted and transmitted beam give rise to an interference fringe pattern in the final

real-space image. For a perfect crystal (but not, in general, for imperfect crystals) the fringes are parallel to, and have the same spacing as, the crystal lattice planes giving the diffracted beam. The maxima or minima of the fringe intensity distribution do not, in general, coincide with the planes of atoms. The fringe positions vary with crystal thickness and with the defocus of the objective lens. Contrast reversals occur periodically as the focus is changed and the series of self-images known as 'Fourier images' (Cowley & Moodie, 1960) are formed.

For small-unit-cell materials, a relatively small number of strong inner reflections may be produced when the incident beam is nearly parallel to a zone axis. Two-dimensional interference fringe patterns are then formed and the relative phases of the various Fourier-component fringes vary strongly with crystal thickness and defocus. Except for very thin crystals, second-order interference effects between diffracted beams can be important and these can lead to severe complications in the interpretation of the images. For example, it is possible to produce 'dumbbell' images for various thicknesses and defocus values which seem to show the separation of two very close rows of atoms when these atom rows cannot be resolved under ideal WPOA conditions (Smith & O'Keefe, 1983).

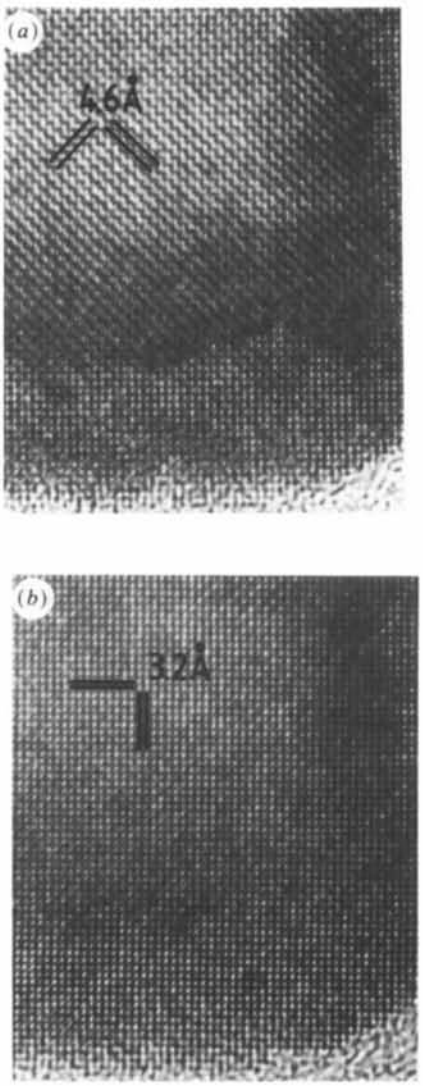

Fig. 9. (*a*) Wedge-shaped crystal of rutile in [001] projection at 500 kV showing anomalous 4·6 Å lattice fringes. (*b*) Same crystal after slight adjustment (<0·2 mrad) of beam tilt.

These appearances are artefacts of the dynamical scattering process. It is only for very thin crystals, imaged close to the optimum defocus (see Fig. 2), that it is possible to relate the image directly to a projection of the crystal structure, and then only within the interpretable resolution limit. Even then it is advisable to make detailed comparisons with computed images in order to ensure the correctness of the image interpretation. For less-ideal conditions, it is usually advisable, and sometimes essential (*e.g.* Smith, Bursill & Wood, 1983) to resort to a detailed matching of the contrast variations throughout an entire through-focus series before accepting a proposed structural model as correct.

Given that the basis of image interpretation is a comparison between theoretical and observed image intensities, rather than a reliance on an intuitive understanding of the image as a representation of atom positions, there would seem to be no reason, in principle, why the information derived from the image should be limited to the 'interpretable resolution' rather than the 'instrumental resolution', which may be considerably better. There have, in practice, been several cases where information beyond the usually defined resolution limit has been derived in a reliable manner; an example was the determination of the structure of platelets in diamond (Barry, Bursill & Hutchison, 1983). In general, however, the difficulties involved in extending the effective resolution by these methods are considerable because of the number of instrumental parameters involved, and because the accuracy with which they must be known increases rapidly as the resolution limit is improved. Without the practical guidelines developed on the basis of reference to recognizable images, the experimental problems become severe. Most of the efforts to interpret images to resolutions beyond the interpretable resolution limit have been restricted to special cases such as the very thin weakly scattering objects for which the WPOA is applicable.

Image reconstruction and restoration

The practical limitations which apply to holography with the STEM also apply to reconstructions

based on out-of-focus CTEM images formed with parallel coherent radiation. Such images may be considered as in-line holograms since their intensities reflect the coherent addition of the complex amplitudes of the scattered radiation with the strong directly transmitted reference wave. In general, however, the images cannot be used to determine the object wave function unless the weak-phase approximation remains valid since any dynamical scattering fails to preserve the phase information of the image (Misell, 1978). There are several possibilities for provision of an off-axis reference wave for the purposes of holography within the CTEM, such as an electrostatic or magnetic biprism or complementary half-plane objective apertures (Misell, 1978). Until recently, none of these methods had succeeded in providing more information about the object than was already available from the normal HREM image.

An alternative approach in attempting to determine crystal structure, or the detailed morphology of a crystal defect, is to carry out image restoration using digitization and computer analysis methods. Spatial averaging can, of course, be applied to a single image to enhance prominent periodicities or to suppress noise but the averaged image will still lack information about the object corresponding to zeros in the PCTF and details of aperiodic defects such as interfaces or dislocations will be blurred out. An object reconstruction based instead on a focal series (Schiske, 1973) enables the effects on the image of gaps in the PCTF to be removed once the respective PCTFs have been determined, and the overall signal-to-noise ratio is also improved. Moreover, the phase component of the image can be readily separated from the amplitude (modulus) component and it is interesting, though not yet properly understood, that the latter still appears to represent accurately the object structure despite the presence of considerable dynamical diffraction (Saxton & Smith, 1985). Latest results indicate that the projections of atomic columns in some materials can be reliably located to within about one-twentieth of the microscope resolution limit following a series restoration; otherwise, the accuracy of location is perhaps three times worse, though still much better than the resolution limit, even for images recorded close to the optimum defocus position (Saxton & Smith, 1985).

Special-purpose microscopy

For many investigations, the type of specimen to be studied, or the conditions under which the observations must be made, preclude the attainment of high resolution. For most organic and biological specimens, and for many inorganic materials, the sensitivity to radiation damage is such as to preclude the use of the incident-beam intensities which are normally required for the observation and recording of high-resolution images. Spatial averaging of the intensities from many unit cells of an extended periodic sample, using either optical or digital methods, represents an effective means to lower the average electron dose received per unit cell (Kuo & Glaeser, 1975), and hence to reduce the damage incurred. This method is obviously not feasible for aperiodic objects or structural defects. At temperature extremes, difficulties arise through mechanical instabilities and thermal drift of the specimen, although resolutions of about 10 Å have been reported for specimens at 1373 K by Moodie & Warble (1975) and resolutions of better than 3 Å have been attained at liquid-helium temperatures by Gibson, Chen & McDonald (1983) and Aoki *et al.* (1986). Correction of image drift using an on-line computer-feedback control system has been demonstrated (Atkin, Erasmus & Smith 1982) but no workable system yet appears to have been incorporated into any commercial microscope.

For studies of solid-gas reactions with gas pressures of more than 10^{-3} Pa, it is necessary to mount specimens in an environmental cell in which the pressure is maintained by the use of electron-transparent thin windows or else by differential pumping and small apertures. Scattering of the electron beam by gas molecules, or by the thin windows, then degrades the contrast of any high-resolution image detail. For specimens which cannot be made with thicknesses less than several hundred ångströms, either because the appropriate thinning techniques are not available or because thinning would destroy essential features of the specimen, the image resolution is limited by the strong multiple scattering of electrons within the material. Microscopes with higher accelerating voltages potentially offer some improvements in this respect, basically because of lower scattering cross sections. Various proposals have been made for recovering useful structural information from thicker specimens (Saxton, 1980), but these have so far only been marginally successful at best. It currently appears that little further progress in such structure refinements can be expected until either inelastic electron scattering is eliminated from the image by energy filtering or until some reliable means can be found to incorporate it into image simulations (Stobbs & Saxton, 1987).

Studies of surface structure

Several TEM methods have recently been developed which allow crystal surfaces to be imaged with atomic resolution in at least one dimension. Initial results suggest that these studies should have a steadily increasing impact on our knowledge and understanding of surfaces and surface phenomena (Smith, 1986*a*; Cowley, 1987).

The image contrast in CTEM is normally dominated by the interior structure of the thin-film speci-

men but, for crystalline films which have no internal defects, all the diffracted beams from the bulk crystal structure can be prevented from contributing to the image by an appropriate choice of the objective aperture size. The only scattering which contributes to the image contrast then originates either from surface structures which are different from the bulk or, in the case of f.c.c. metals and some other materials, because the crystal thickness is a non-integral number of unit cells, leading to 'forbidden' reflections (Goodman & Moodie, 1974). This surface scattering is weak so that the contrast of bright-field images is usually low. Better contrast is provided by dark-field imaging using only the diffracted beams from surface layers, although lengthy exposure times are required. This method has been applied to the study of surface layers on gold (111) faces (Cherns, 1974), to single-atom-high steps on graphite and silicon by Iijima (1981) and to the growth of single and multiple layers of Ag on MoS_2 by Takayanagi (1983). Bulk (200) reflections have been filtered *a posteriori* from high-resolution images by computer processing, revealing the 'forbidden' [110] surface periodicities (Krakow, 1979).

Periodic surface structures which differ in periodicity from the bulk lattice give weak superstructure spots in transmission high-energy electron diffraction (HEED) patterns. It has been established that within well defined limits the scattering from the surface layers may be interpreted by use of the simple kinematical approximation (Spence, 1983). Hence the surface superstructure diffraction-spot intensities may be utilized as a basis for structure analysis using methods previously developed for X-ray diffraction. An outstanding example is the recent determination of the structure of the Si(111) 7×7 periodic surface reconstruction (Takayanagi, Tanishiro, Takahashi & Takahashi, 1985).

Steps of single-atom height on relatively flat surfaces of bulk crystals can be imaged with high contrast by the use of the reflection electron microscopy (REM) technique or the scanning-beam equivalent (SREM). REM images are formed from the diffracted beams within the RHEED patterns which result when the electron beam is incident on the surface at a grazing angle of a few degrees. The images are severely foreshortened in the beam direction because of the grazing incidence but they may have resolutions of better than 10 Å in directions perpendicular to the beam (Hsu, 1983). Notable examples of application of the method include studies of the surface structure and the formation of surface superstructures on silicon crystals by Yagi and co-workers (Tanishiro, Takayanagi & Yagi, 1983) and the studies of metal surfaces by Hsu & Cowley (1983).

The ultimate high-resolution capability of modern HREM instruments has been applied to the characterization of surfaces by means of the profile imaging technique. Images from the edges of thin films or small particles show projections of the structure along the rows of atoms lying in, or near to, the surface. The initial studies at atomic resolution by Marks & Smith (1983) which revealed a short 2×1 reconstruction of the Au(110) surface, have been followed by further studies of a variety of materials, mostly oxides, as well as atomic motion on the surfaces of a number of metals and oxides (Smith, Bursill, Bovin, Petford-Long & Ye, 1986).

Beam-induced reactions

The irradiation of the specimen by the intense electron beam required for HREM is often regarded as a serious hindrance to the collection of structural information on the atomic scale since it may rapidly destroy the crystallinity, change the composition or induce phase changes in otherwise stable inorganic systems (Hobbs, 1984). The effects of irradiation may be minimized by averaging techniques where applicable, or by the use of highly efficient detection devices. The fundamental limit on achievable information will be reached when image recording starts with the first electrons to traverse the specimen and all electrons are detected with 100% efficiency.

Alternatively, electron irradiation may be used for studying reaction mechanisms and the progress of phase changes, since the radiation-induced changes may be sufficiently close to those induced thermally to allow useful analogies to be drawn. In other contexts the irradiation effects themselves may be of interest because the behavior of solids under intense ionizing radiation is relevant for an increasing number of technologically and scientifically important systems.

In recent studies, observations at atomic resolution have been made of radiation-induced transitions from oxides to metals (Long & Petford-Long, 1986), from metals to oxides (Lodge & Cowley, 1984), from crystalline to amorphous materials (Cherns, Hutchison, Jenkins & Hirsch, 1980) and from amorphous to crystalline materials (Parker & Sinclair, 1986). The occurrence of electron-beam-stimulated desorption of various anion species from near-surface regions has also been summarized (Smith, 1986*b*).

Developments in instrumentation

Further progress towards wide-ranging applications of HREM in surface science can only be achieved when the conditions of the surfaces are better controlled than is possible in standard electron microscopes. The residual vacuum levels (10^{-5} Pa or more) and the presence of carbonaceous contamination adversely affect the imaging of surface structure for many specimens, and meaningful studies of most surface reactions are not feasible. The high-temperature high-vacuum studies of clean silicon sur-

faces (Osakabe, Tanishiro, Yagi & Honjo, 1981) were only made possible by the use of a specially modified commercial microscope. Several electron microscopes have recently been designed specifically for HREM studies of specimens prepared and held in ultra-high vacuum ($\sim 10^{-8}$ Pa) (*e.g.* Yagi *et al.*, 1982). Adequate provision can be made for *in situ* treatment (heating, evaporation *etc.*) of the surfaces, and for concurrent microanalysis by various surface-sensitive techniques. The knowledge and insights which should come from studying surface structure and the progress of surface reactions at atomic resolution will undoubtedly lead to rapid advances in this area.

The combination of small probes and the absence of post-specimen lenses close to the sample makes it straightforward in the STEM to detect a variety of useful analytical signals from local regions. The need for combined high-resolution and microanalysis facilities for many materials-science problems has been cogently argued by Stobbs (1983). However, the demand for ultimate performance in the CTEM means that less space around the sample is generally available, and it becomes very difficult, for example, to provide a reasonable take-off angle for X-ray detection and microanalysis. The suggested alternative is to add the capability for electron energy-loss spectroscopy (EELS) since an EELS device at the beam of the microscope column does not interfere with the HREM imaging performance. Moreover, with the recent implementation of parallel detection capabilities to the spectrometer (Shuman & Kruit, 1985), a high-quality spectrum can be acquired in a matter of seconds, rather than minutes, so that the EELS technique has reached a new plateau of sensitivity yet to be fully evaluated. Finally, high-resolution energy-filtered images can be recorded with the parallel-detection systems (Krivanek & Ahn, 1986) so that further progress on structure refinement from thicker crystals can be anticipated to follow (Stobbs & Saxton, 1987).

The opportunities for microprocessor or computer control of many microscope operations have yet to be fully explored. The recent changeover from analog to digital electronics means, for example, that the procedure of stepping the STEM probe across a sample whilst simultaneously recording microdiffraction patterns and microanalytical signals can be made more systematic. In the CTEM, the provision of an on-line signal to the computer, *via* an image pickup system and framestore, facilitates correction of the incident-beam misalignment, as well as the adjustment of the objective-lens defocus and astigmatism (Saxton, Smith & Erasmus, 1983). Correction of image drift has been demonstrated as feasible (Atkin, Erasmus & Smith, 1982). The accuracy and reliability with which these functions can be carried out under computer control generally exceeds the capabilities of experienced operators. The improved convenience and the prospect for better quantitative data represent powerful driving forces for the widespread implementation of digital microscope control in the near future.

Table 1. *Variation of interpretable resolution as a function of accelerating voltage and the spherical aberration coefficient*

kV	λ (Å)	C_s (mm)	δ (Å)
100	0·0370	0·7	2·9
200	0·0251	0·8	2·2
300	0·0197	0·9	1·90
400	0·0164	1·0	1·70
600	0·0126	1·5	1·55
1000	0·0087	2·3	1·30
2000	0·0050	4·0	0·99

Prospects for resolution improvement

There are several alternatives for extending the existing limits on image resolution. An obvious possibility is to redesign the objective lens in order to lower the value of the spherical aberration coefficient. In recent years commercial manufacturers have put considerable effort into optimizing objective-lens design so that it currently seems unlikely that the C_s values listed in Table 1 can improve significantly. Moreover, because of the weak dependence of the resolution limit δ on the C_s value, a factor of 2 change in C_s leads only to about 20% change in δ. The specimen stages associated with these lenses are already rather restricted in their available tilting facilities, with limits of $\pm 10°$ or less being common for the lower-voltage instruments because of the heavily confined space. Zero tilt capability is not a viable option for studying crystalline materials. In summary, other avenues should be explored.

An increase in the accelerating voltage leads to shorter electron wavelengths but, because of the strong magnetic fields needed to focus higher-energy electrons, saturation in pole-piece material causes a steady increase in aberration coefficients. The net effect of an increase in electron energy is, however, a steady improvement in the resolution figure, as illustrated in Table 1.

The present limitations suggested by the table may well be modified in the future by the advent of convenient superconducting lenses. Electron microscopes employing liquid-helium-cooled superconducting lens coils have shown good resolution but are necessarily inconvenient in their operation (Lefranc, Knapek & Dietrich, 1982). They have been used mainly in applications for which it is an advantage to hold the specimen also at low temperatures as in studies of biological materials with reduced radiation damage or in studies of low-temperature phase changes of inorganic materials. If superconducting lenses operating at liquid-nitrogen temperatures or above can be made to give higher mag-

netic fields and stronger lenses, the limitations due to saturation of pole-piece material will be avoided, with some improvement of resolution, especially for higher voltages.

The use of superconductors may also assist with the technical problems of maintaining the stabilities of the electrical systems but not necessarily with the problems of mechanical stability. However, the nature of the electron–specimen interaction imposes a more fundamental restriction. Above a well defined threshold voltage, which is characteristic of each specific material, the electrons of the incident beam have sufficient energy to cause a ballistic or 'knock-on' displacement of the constituent atoms of the material. The rate of atomic displacement is accentuated under the high-electron-dose conditions needed for recording the high-resolution images, and it becomes impossible to determine the atomic configurations around some crystal defects because of the simultaneous rapid loss of material. The need for a balance between radiation damage and attainable resolution necessitates a flexible compromise on the optimum operating voltage chosen for high-resolution imaging of different specimens (Gronsky & Thomas, 1983).

The possibility of correcting for the third-order spherical and chromatic aberration coefficients of the objective lens has attracted intermittent attention over the years [for details, see Koops (1978) and Glaeser (1979)], with the latest suggestion for correcting C_s involving the use of the sextupole–round lens combination (Crewe & Kopf, 1980). A major problem in the realization of a viable corrector appears to have been the excessively stringent mechanical and electrical tolerances – which do not appear so unreasonable these days. A breakthrough in aberration correction would certainly have a dramatic impact on the current stuatus of HREM, although it is just as well to be aware that further practical problems would then follow from a reduced depth of focus, the requirement for greatly improved electrical and mechanical stabilities, the necessity for much greater precision in the determination of operational parameters, including the need for more accurate beam alignment, and the importance of fourth- and fifth-order aberration coefficients.

In some lower-voltage (100–200 kV) instruments, the limit of instrumental resolution is already known to be well beyond that of the interpretable resolution (Smith, Camps & Freeman, 1982). By using a lanthanum hexaboride thermionic cathode or a field-emission source, it should be possible to arrange that the spatial coherence envelope is not limiting the performance (see Fig. 3). Moreover, use of a field-emission gun in the cold-emission mode should, in principle at least, significantly extend the temporal coherence envelope since the intrinsic energy spread is less than 0·8 eV, compared with thermionic sources where 1·5–2·0 eV is common (Troyon, 1976). The possibility therefore exists, as pointed out elsewhere (Humphreys & Spence, 1981), for a marked gain in the overall instrumental limit, perhaps even to better than 1 Å in a 200 kV CTEM. Deconvolution of the effect of the PCTF by using a series restoration, as described above, should then result in a concomitant improvement in the information about the object which can be reliably extracted from the image. Full advantage of these possiblities does not yet appear to have been taken. Marginal gains in resolution were reported by Saxton, Howie, Mistry & Pitt (1977) for images of amorphous silicon and germanium. Kirkland, Siegel, Uyeda & Fujiyoshi (1985) have analyzed images of chlorinated phthalocyanines taking into account deviations from the ideal kinematical single scattering. The images of a platinum–charcoal catalyst analyzed by Saxton (1980) were rendered interpretable by series restoration but the resolution gains were again marginal because of the restrictions imposed by the coherence envelopes. Better instrumentation combined with cheaper and faster computing equipment should lead to significant improvements in the near future (see Hawkes, 1984).

Concluding remarks

The improvement in the resolution achieved with commercial electron microscopes over the past 15 years, from around 3 to about 1·5 Å, has allowed very important advances in the use of HREM to investigate the structures of crystals and their defects, surfaces and interfaces. It is now possible to obtain separate-atom images of a much broader range of materials. Atom positions can be determined with much higher accuracy. A comparable improvement in resolution and an associated increase in the power of the method may be expected in the next 15 years. This advance will probably come mostly through an improvement in the engineering of the electron microscopes, possibly involving superconductor technology, with the use of higher voltages and improved stabilities of the electrical supplies.

The indirect methods for improving the effective resolution by use of image processing, holography and related techniques have had little impact on practical microscopy as yet. It may well be that these methods will gain increasing importance as the digital techniques for instrument control and data processing are developed further. It is already evident that in many cases the derivation of information from electron microscopy is limited by the accuracy with which the relevant experimental parameters of the microscope and of the specimen may be determined and adjusted. Any further improvement of resolution, by any direct or indirect method, will necessarily require greatly increased precision in the control and measurement of such factors as the alignment of the microscope, the aberrations and defocus of the objec-

tive lens, the energy spread and beam divergence of the electron beam, the thickness and orientation of a crystalline specimen and the presence and nature of any surface layers or defects of the crystal.

The damage to the specimen by the incident electron beam imposes an absolute limitation on the amount of information which can be obtained. It is possible that the techniques can be advanced to the stage that all the information concerning the scattering of each incident electron is derived, up to the limits set by the uncertainty principle. This implies a considerable increase in complication and expense of the equipment but will gradually become more feasible technically and more rewarding in terms of results.

Finally, it should be pointed out that some of the most important advances in electron microscopy in the next few years will come not from improvement in resolution but from improvements in the control of specimen environments and from the use of auxiliary techniques. The possibility of preparing and examining specimens in ultra-high vacuum, or a controlled atmosphere, with variable specimen temperature, promises major advances in the study of surface structures and the chemical reactions on surfaces or in thin films, viewed with atomic resolution. Further developments of the microanalytical and microdiffraction techniques will allow the imaging data to be coupled with compositional and crystallographic data from smaller and smaller specimen regions down to clusters of a few atoms. The integration of scanning tunnelling microscopy and other tools such as Auger-electron spectroscopy with electron microscopy, in reflection or transmission, can open up whole new ranges of applications which have scarcely yet been considered (Venables, Smith & Cowley, 1987).

References

AOKI, T., KIHARA, H., HARADA, Y., FUJIYOSHI, Y., UYEDA, N., YAMAGISHI, H., MORIKAWA, K. & MIZUSAKI, T. (1986). In *Electron Microscopy* 1986, edited by T. IMURA, S. MARUSE & T. SUZUKI, Vol. 3, pp. 1827-1828. Tokyo: Japanese Society of Electron Microscopy.

ATKIN, P., ERASMUS, S. J. & SMITH, K. C. A. (1982). In *Electron Microscopy* 1982, Vol. 1, pp. 525-526. Frankfurt: Deutsche Gesellschaft für Elektronenmikroskopie e.V.

BARRY, J. C., BURSILL, L. A. & HUTCHISON, J. L. (1983). *Philos. Mag.* **A48**, 109-121.

BERGER, S. D. & PENNYCOOK, S. J. (1982). *Nature (London)*, **298**, 635-637.

BOURRET, A. & COLLIEX, C. (1982). *Ultramicroscopy*, **9**, 183-189.

BURSILL, L. A. & LIN, P. J. (1985). *Nature (London)*, **316**, 50-51.

CHERNS, D. (1974). *Philos. Mag.* **30**, 549-556.

CHERNS, D., HUTCHISON, J. L., JENKINS, M. L. & HIRSCH, P. B. (1980). *Nature (London)*, **287**, 314-316.

COWLEY, J. M. (1969). *Appl. Phys. Lett.* **15**, 58-59.

COWLEY, J. M. (1980). In *Scanning Electron Microscopy* 1980, vol. 1, edited by O. JOHARI, pp. 61-72. SEM Inc., AMF O'Hare, IL, USA.

COWLEY, J. M. (1981). *Diffraction Physics*, 2nd ed. Amsterdam: North-Holland.

COWLEY, J. M. (1984). *Bull. Mater. Sci.* **6**, 477-490.

COWLEY, J. M. (1987). *Prog. Surf. Sci.* **21**, 209-250.

COWLEY, J. M. & AU, A. A. (1978). *Acta Cryst.* A**34**, 738-743.

COWLEY, J. M. & MOODIE, A. F. (1957). *Acta Cryst.* **10**, 609-619.

COWLEY, J. M. & MOODIE, A. F. (1960). *Proc. Phys. Soc. London*, **76**, 378-384.

COWLEY, J. M., OSMAN, M. A. & HUMBLE, P. (1984). *Ultramicroscopy*, **15**, 311-318.

CREWE, A. V. & KOPF, D. (1980). *Optik (Stuttgart)*, **55**, 1-10.

CREWE, A. V., WALL, J. B. & WELTER, L. M. (1968). *J. Appl. Phys.* **39**, 5861-5868.

ERICKSON, H. P. (1973). *Adv. Opt. Electron Microsc.* **5**, 163-199.

EYRING, L., DUFNER, C., GORAL, J. P. & HALLADAY, A. (1985). *Ultramicroscopy*, **18**, 253-274.

FRANK, J. (1973). *Optik (Stuttgart)*, **38**, 519-536.

GABOR, D. (1948). *Nature (London)*, **161**, 777-778.

GIBSON, J. M., CHEN, C. H. & MCDONALD, M. L. (1983). *Phys. Rev. Lett.* **50**, 1403-1405.

GLAESER, R. M. (1979). *J. Microsc. (Oxford)*, **117**, 77-91.

GOODMAN, P. & MOODIE, A. F. (1974). *Acta Cryst.* A**30**, 280-290.

GRONSKY, R. & THOMAS, G. (1983) In *41st Ann. Proc. Electron Microscopy Society of America*, edited by G. W. BAILEY, pp. 310-311. San Francisco: San Francisco Press.

HAWKES, P. W. (1984). In *Quantitative Electron Microscopy*, edited by J. N. CHAPMAN & A. J. CRAVEN, Chap. 10, pp. 351-397. Scottish Univs. Summer School in Physics, Edinburgh, Scotland.

HIRAGA, K., HIRABAYASHI, M., INOUE, A. & MATSUMOTO, T. (1985). *Sci. Rep. Res. Inst. Tohoku Univ.* **32**, 309-314.

HOBBS, L. W. (1984). In *Quantitative Electron Microscopy*, edited by J. N. CHAPMAN & A. J. CRAVEN, Chap. 11, pp. 399-445. Scottish Univs. Summer School in Physics, Edinburgh, Scotland.

HSU, T. (1983). *Ultramicroscopy*, **11**, 167-172.

HSU, T. & COWLEY, J. M. (1983). *Ultramicroscopy*, **11**, 239-250.

HUMPHREYS, C. J. & SPENCE, J. C. H. (1981). *Optik (Stuttgart)*, **58**, 125-142.

HUTCHISON, J. L. (1985). *Ultramicroscopy*, **18**, 349-354.

IIJIMA, S. (1981). *Ultramicroscopy*, **6**, 41-52.

IIJIMA, S. & ICHIHASHI, T. (1986). *Phys. Rev. Lett.* **55**, 616-619.

IMESON, D., MILNE, R. H., BERGER, S. D. & MCMULLAN, D. (1985). *Ultramicroscopy*, **17**, 243-249.

KANG, Z. C., SMITH, D. J. & EYRING, L. (1986). *Surf. Sci.* **175**, 684-692.

KIRKLAND, E. J., SIEGEL, B. M., UYEDA, N. & FUJIYOSHI, Y. (1985). *Ultramicroscopy*, **17**, 87-104.

KONNERT, J. & D'ANTONIO, P. (1986). *Ultramicroscopy*, **19**, 267-277.

KOOPS, H. (1978). In *Electron Microscopy* 1978, edited by J. M. STURGESS, Vol. 3, pp. 185-196. Toronto: Microscopical Society of Canada.

KRAKOW, W. (1979). *Ultramicroscopy*, **4**, 55-76.

KRIVANEK, O. L. & AHN, C. (1986). In *Electron Microscopy* 1986, edited by T. IMURA, S. MARUSE & T. SUZUKI, Vol. 1, pp. 519-520. Tokyo: Japanese Society of Electron Microscopy.

KUO, I. & GLAESER, R. M. (1975). *Ultramicroscopy*, **1**, 53-66.

LEFRANC, G., KNAPEK, E. & DIETRICH, I. (1982). *Ultramicroscopy*, **10**, 111-124.

LIN, L. A. & COWLEY, J. M. (1986). *Ultramicroscopy*, **19**, 179-190.

LODGE, E. A. & COWLEY, J. M. (1984). *Ultramicroscopy*, **13**, 215-226.

LONG, N. J. & PETFORD-LONG, A. K. (1986). *Ultramicroscopy*, **20**, 151-160.

MARKS, L. D. & SMITH, D. J. (1983). *Nature (London)*, **303**, 316-318.

MISELL, D. L. (1978). In *Advances in Optical and Electron Microscopy*, edited by V. E. COSSLETT & R. BARER, Vol. 7, pp. 185-279. London: Academic Press.

MONOSMITH, W. B. & COWLEY, J. M. (1983). *Ultramicroscopy*, **12**, 177-183.

MOODIE, A. F. & WARBLE, C. E. (1975). In *Sintering and Catalysis*, edited by G. C. KUCZYNSKI, pp. 1-16. New York: Plenum.

OSAKABE, N., TANISHIRO, Y., YAGI, K. & HONJO, G. (1981). *Surf. Sci.* **109**, 353-366.
PARKER, M. A. & SINCLAIR, R. (1986). In *Electron Microscopy* 1986, edited by T. IMURA, S. MARUSE & T. SUZUKI, Vol. 2, pp. 991-992. Tokyo: Japanese Society of Electron Microscopy.
SAXTON, W. O. (1978). *Computer Techniques for Image Processing in Electron Microscopy.* New York: Academic Press.
SAXTON, W. O. (1980). *J. Microsc. Spectrosc. Electron.* **5**, 665-674.
SAXTON, W. O., HOWIE, A., MISTRY, A. & PITT, A. (1977). *Inst. Phys. Conf. Ser.* No. 36, pp. 119-122.
SAXTON, W. O. & SMITH, D. J. (1985). *Ultramicroscopy*, **18**, 39-48.
SAXTON, W. O., SMITH, D. J. & ERASMUS, S. J. (1983). *J. Microsc. (Oxford)*, **130**, 187-201.
SCHISKE, P. (1973). In *Image Processing and Computer-Aided Design in Electron Optics*, edited by P. W. HAWKES, pp. 82-90. London: Academic Press.
SELF, P. G., O'KEEFE, M. A., SPARGO, A. E. & BUSECK, P. R. (1984). *Ultramicroscopy*, **11**, 35-62.
SHUMAN, H. & KRUIT, P. (1985). *Rev. Sci. Instrum.* **56**, 231-239.
SMITH, D. J. (1985). *J. Vac. Sci. Technol.* **B3**, 1563-1566.
SMITH, D. J. (1986*a*). In *Chemistry and Physics of Solid Surfaces* VI, edited by R. VANSELOW & R. HOWE, Chap. 15. Berlin: Springer-Verlag.
SMITH, D. J. (1986*b*). *Surf. Sci.* **178**, 462-474.
SMITH, D. J., BURSILL, L. A., BOVIN, J.-O., PETFORD-LONG, A. K. & YE, H. Q. (1986). *Surf. Interface Anal.* **10**, 135-141.
SMITH, D. J., BURSILL, L. A. & WOOD, G. J. (1983). *J. Solid State Chem.* **50**, 51-69.
SMITH, D. J., BURSILL, L. A. & WOOD, G. J. (1985). *Ultramicroscopy*, **16**, 19-32.
SMITH, D. J., CAMPS, R. A. & FREEMAN, L. A. (1982). *Inst. Phys. Conf. Ser.* No. 61, pp. 381-386.
SMITH, D. J. & MARKS, L. D. (1985). *Ultramicroscopy*, **16**, 101-114.
SMITH, D. J. & O'KEEFE, M. A. (1983). *Acta Cryst.* **A39**, 139-148.
SMITH, D. J., PETFORD, A. K., WALLENBERG, L. R & BOVIN, J.-O. (1986). *Science*, **233**, 872-875.
SMITH, D. J., SAXTON, W. O., O'KEEFE, M. A., WOOD, G. J. & STOBBS, W. M. (1983). *Ultramicroscopy*, **11**, 263-281.
SPENCE, J. C. H. (1983). *Ultramicroscopy*, **11**, 117-124.
STOBBS, W. M. (1983). *J. Microsc. (Oxford)*, **131**, 47-53.
STOBBS, W. M. & SAXTON, W. O. (1987). *J. Microsc. (Oxford)*. In the press.
TAKAYANAGI, K. (1983). *Jpn. J. Appl. Phys.* **22**, L4-6.
TAKAYANAGI, K., TANISHIRO, Y., TAKAHASHI, S. & TAKAHASHI, M. (1985). *Surf. Sci.* **164**, 367-392.
TANISHIRO, Y., TAKAYANAGI, K. & YAGI, K. (1983). *Ultramicroscopy*, **11**, 95-102.
THON, F. (1971). In *Electron Microscopy in Materials Science*, edited by U. VALDRE, pp. 570-625. New York and London: Academic Press.
TONOMURA, A. (1986). In *Electron Microscopy* 1986, edited by T. IMURA, S. MARUSE & T. SUZUKI, Vol. 1, pp. 9-14. Tokyo: Japanese Society of Electron Microscopy.
TROYON, M. (1976). *Optik (Stuttgart)*, **46**, 439-450.
VENABLES, J. A., SMITH, D. J. & COWLEY, J. M. (1987). *Surf. Sci.* **181**, 235-249.
WILSON, A. R., SPARGO, A. E. & SMITH, D. J. (1981). *Optik (Stuttgart)*, **61**, 63-78.
YAGI, K., TAKAYANAGI, K., NAGAKURA, S., KOBAYASHI, K., HONJO, G., KUBOZOE, M., SHII, K., MATSUI, I., KATAGIRI, S. & TANAKA, T. (1982). In *Electron Microscopy* 1982, Vol. 1, pp. 375-376. Frankfurt: Deutsche Gesellschaft für Elektronenmikroskopie e.V.
ZEMLIN, F., WEISS, K., SCHISKE, P., KUNATH, W. & HERRMANN, K.-H. (1978). *Ultramicroscopy*, **3**, 49-60.

Acta Cryst. (1987). **A43**, 751-763

Optimal Symbolic Phase Determination

BY RENÉ PESCHAR AND HENK SCHENK

Laboratory of Crystallography, University of Amsterdam, Nieuwe Achtergracht 166, 1018 *WV Amsterdam, The Netherlands*

(*Received* 15 *October* 1986; *accepted* 21 *May* 1987)

Abstract

A systematic method of phase determination is presented inspired by the dynamic-programming principle. In this new procedure the starting set and the best phasing sequence are determined while executing the symbolic phase determination itself. Special attention is given to the way in which statistical weights for symbolic phase indications can be calculated. Test results show that the new procedure leads to considerable improvements over the phase-determination procedures based on the convergence procedure currently available.

Introduction

The phase problem is often tackled successfully by a default run of a direct-method structure-determination program, such as *SIMPEL* (Overbeek & Schenk, 1978; Schenk & Kiers, 1985), *MULTAN* (Main, 1985), *SHELX* (Sheldrick, 1985) or *GENTAN* (Hall, 1985). However, the structure is not always found immediately. Although the reasons for failure may vary, the user of a program should at least be guaranteed that under the given basic probabilistic assumptions the best possible phase determination is carried out; that is, the chance of obtaining the correct solu-

0108-7673/87/060751-13$01.50